



HAL
open science

Turbulent transition in Rayleigh-Bénard convection with Fluorocarbon

Lucas Méthivier, Romane Braun, Francesca Chillà, Julien Salort

► **To cite this version:**

Lucas Méthivier, Romane Braun, Francesca Chillà, Julien Salort. Turbulent transition in Rayleigh-Bénard convection with Fluorocarbon. 2021. hal-03261081v1

HAL Id: hal-03261081

<https://hal.science/hal-03261081v1>

Preprint submitted on 15 Jun 2021 (v1), last revised 8 Oct 2021 (v3)

HAL is a multi-disciplinary open access archive for the deposit and dissemination of scientific research documents, whether they are published or not. The documents may come from teaching and research institutions in France or abroad, or from public or private research centers.

L'archive ouverte pluridisciplinaire **HAL**, est destinée au dépôt et à la diffusion de documents scientifiques de niveau recherche, publiés ou non, émanant des établissements d'enseignement et de recherche français ou étrangers, des laboratoires publics ou privés.

Turbulent transition in Rayleigh-Bénard convection with Fluoro-carbon

LUCAS MÉTHIVIER¹, ROMANE BRAUN¹, FRANCESCA CHILLÀ¹ and JULIEN SALORT¹

¹ *Univ Lyon, ENS de Lyon, CNRS, Laboratoire de Physique, Lyon, France*

Abstract – We present measurements of the heat-transfer and the velocity field in two Rayleigh-Bénard cells (aspect ratios 1 and 2). We use Fluorinert FC770 as the working fluid, up to a Rayleigh number 2×10^{12} . The velocity field is inferred from sequences of Shadowgraph pattern using a Correlation Image Velocimetry (CIV) algorithm. Indeed the large number of plumes, and their small characteristic scale, make it possible to use the Shadowgraph pattern produced by the thermal plumes in the same manner as particles in Particle Image Velocimetry (PIV). The method is validated in water against PIV, and yield identical wind velocity estimates. The joint heat-transfer and velocity measurements allow to compute the scaling of the kinetic dissipation rate which features a transition from a laminar $Re^{5/2}$ scaling to a turbulent Re^3 scaling. We propose that the turbulent transition in Rayleigh-Bénard convection is controlled by a threshold Péclet number rather than Rayleigh number, which may explain the apparent discrepancy in the literature regarding the “ultimate” regime of convection.

Introduction. – Turbulent thermal convection is a modern and important problem involved in a lot of practical situations and linked to environmental challenge. Natural flows are indeed difficult to characterise and physicists use often some model systems, such as the Rayleigh-Bénard flows which can mimic a lot of situations and are easy to manage in laboratory. The definition of Rayleigh-Bénard (RB) flow is a fluid layer confined in a cell of characteristics height h on which a difference of temperature $\Delta T = T_{\text{bottom}} - T_{\text{top}}$ is applied to destabilise the flow, so that $T_{\text{bottom}} > T_{\text{top}}$. The non-dimensional parameters characterising the forcing are the Rayleigh number

$$Ra = \frac{g\alpha\Delta Th^3}{\nu\kappa}, \quad (1)$$

and the Prandtl number

$$Pr = \frac{\nu}{\kappa}, \quad (2)$$

where g is de gravity acceleration, α is the thermal expansion coefficient, ν is the kinematic viscosity and κ the thermal diffusivity, coupled with the aspect ratio $\Gamma = D/h$ where D is the horizontal dimension of the cell.

One of the response parameter is the non-dimensional heat transport, the Nusselt number,

$$Nu = \frac{Qh}{\lambda\Delta T}, \quad (3)$$

where Q is the heat flux injected in the cell, and λ the thermal conductivity. The other important parameter is the Reynolds number

$$Re = \frac{UH}{\nu}, \quad (4)$$

where U is a typical velocity and H a typical scale. As clearly shown in the literature [1,2], the RB flow is largely inhomogeneous and the velocity can change between one place or another of the cell, the definition of H can depend on the place in the cell as well. A point arouse about the scaling laws that can be built as function of the Rayleigh number. To have this kind of discussion, measurements of velocity must be realised in several part of the flow and at different Rayleigh numbers. Two techniques have essentially been used till now: optical measurements such as Laser-Doppler Velocimetry [3], Particle Image Velocimetry (PIV) [4,5] or Lagrangian tracking [6,7]; or the measurement of correlation time delay between two probes in a particular point [8–11], recently a measurement of tracking of plumes from Shadowgraph pattern have been also introduced [12]. In this letter, we introduce a really cheap and easy to manage method, to get an estimate for the full velocity field. Once this technique is introduced, we will discuss the estimated Reynolds numbers, and their scaling. At the end we will discuss the friction coefficient, and how it relates to the turbulent transition.

Experimental set-up. – We are using in this study two parallelepiped Rayleigh-Bénard convection cells with different aspect ratios. The first, of aspect ratio $\Gamma = 1$, with dimensions $41.5 \text{ cm} \times 10.5 \text{ cm} \times 41.5 \text{ cm}$, is the same cell as previously used [12]. The second is identical but was fitted with smaller glass walls of height 20 cm. Its aspect ratio is $\Gamma = 2$. For both cells, the depth is 4 time smaller than the length so the flow is quasi bi-dimensional.

The cells are made with glass to allow optical measurements with better quality than PMMA which yields spurious gradients of optical index. The plates are smooth and made of copper with a thin layer of nickel. The bottom plate is heated with a constant power. The top plate is cooled by a circulation of ethylene-glycol mixture, regulated by a Lauda Variocool chiller. The convection cell is placed inside a PMMA box, thermally regulated at the same temperature as the bulk of the flow. The aim is to reduce the heat losses while keeping the optical access.

The working fluid is Fluorinert FC770 (produced by 3M), which allows to reach higher Rayleigh numbers than those we had in the same apparatus with deionized water [5]. To compute the non-dimensional parameters, accurate estimates of the physical properties of the fluids are required. While they are well known for deionized water, it is not the case for FC770. Previous studies using FC770, such as [13], used the physical properties at 25°C provided by the manufacturer. However, a higher working temperature (40°C) allows to increase the temperature difference, and span a wider range of Rayleigh number. Additionally, the temperature dependence of the physical parameters is useful to estimate the deviation from the Boussinesq approximation. It is therefore difficult to compare the Rayleigh and Nusselt numbers obtained in FC770 with other data from the literature without better estimates of the fluid properties.

Therefore, we got the physical parameters measured by Flucon GmbH, see table 1. However, special care must be taken regarding the thermal conductivity, λ . Indeed, most commercial apparatus have not been designed with a fluid such as FC770 which has both low thermal conductivity and low viscosity, and their design produce spurious natural convection. That is why we performed our own measurements of the thermal conductivity using a TCi thermal conductivity analyzer from C-Therm technologies inside a temperature regulated chamber. In this configuration, the measurement is performed on a thin film of liquid, and not with a heated wire. We find the following fit for $\lambda(T)$, which we use in the remainder of the paper,

$$\lambda(T) = \lambda_0 + (\partial_\theta \lambda)\theta, \quad (5)$$

where $\lambda_0 = 0.1114 \text{ W/m/K}$ is the thermal conductivity at 0°C , $\partial_\theta \lambda = 3 \times 10^{-4} \text{ W/m/K/}^\circ\text{C}$, and θ is the temperature in $^\circ\text{C}$. This value of λ is quite different from the estimate from the manufacturer, $\lambda_{3M} = 0.063 \text{ W/m/K}$ at 25°C . It is unclear how spurious convection bias the measurement, as it depends on details of the apparatus which are

Table 1: Physical properties of FC770 measured by Flucon GmbH.

T [$^\circ\text{C}$]	ρ [kg/m^3]	c_p [K/kg/K]	η [Pas]
-10.0	1890.3	932.2	3.0407×10^{-3}
-5.0	1876.6	942.6	2.6885×10^{-3}
0.0	1863.5	959.2	2.3813×10^{-3}
5.0	1849.4	967.0	2.1223×10^{-3}
10.0	1836.7	979.2	1.9154×10^{-3}
15.0	1822.8	991.6	1.7393×10^{-3}
20.0	1809.8	999.5	1.5783×10^{-3}
25.0	1795.9	1007.4	1.4407×10^{-3}
30.0	1782.1	1023.0	1.3364×10^{-3}
35.0	1769.1	1032.7	1.2236×10^{-3}
40.0	1754.9	1048.6	1.1397×10^{-3}
45.0	1741.7	1055.2	1.0585×10^{-3}
50.0	1728.6	1068.7	9.9312×10^{-4}
55.0	1714.4	1071.8	9.2496×10^{-4}
60.0	1700.8	1085.6	8.7276×10^{-4}
65.0	1687.3	1093.8	8.2490×10^{-4}
70.0	1673.8	1102.0	7.7859×10^{-4}
75.0	1660.5	1115.9	7.3521×10^{-4}
80.0	1647.2	1123.7	6.9451×10^{-4}
85.0	1633.0	1135.4	6.6369×10^{-4}
90.0	1619.5	1154.2	6.3422×10^{-4}
95.0	1606.4	1160.8	6.0256×10^{-4}

not publicly available. As can be seen in Fig 1, our Nusselt numbers are a bit below the values of the GL model. They would however be much higher than the GL model if λ_{3M} was used instead. It is possible that our measurement with the TCi thermal conductivity analyser slightly overestimates λ . The phenomenological value of λ that would offset our heat-transfer data so that it matches the prediction of the GL model is $\lambda_{\text{GL}} = 0.0945 \text{ W/m/K}$ at 25°C .

The heat transfer measurements are reported in table 2 for both aspect ratios. As can be seen in Figure 1, the scaling law for the Nusselt number obtained with FC770 is close to $Ra^{1/3}$, up to $Ra = 2 \times 10^{12}$, in fair agreement with the results from He, et al [14], as well as the Grossmann-Lohse model [15]. However, it is possible that the Nusselt numbers at the highest Ra show an increase, but it is not possible to conclude, as the start of this increase would lie at the very end of our Rayleigh number range. The puzzle remains however why it seems to be in disagreement with the data from Chavanne, et al. [16], and from Niemela, et al. [17, 18].

The interpretation proposed by Chavanne, et al. [16] to explain the heat-transfer enhancement that they report, is a laminar turbulent transition of the boundary layer, which yields the inertial regime predicted by Kraichnan [19]. This interpretation was backed by two observations: (i) a transition for the dissipated power from a lam-

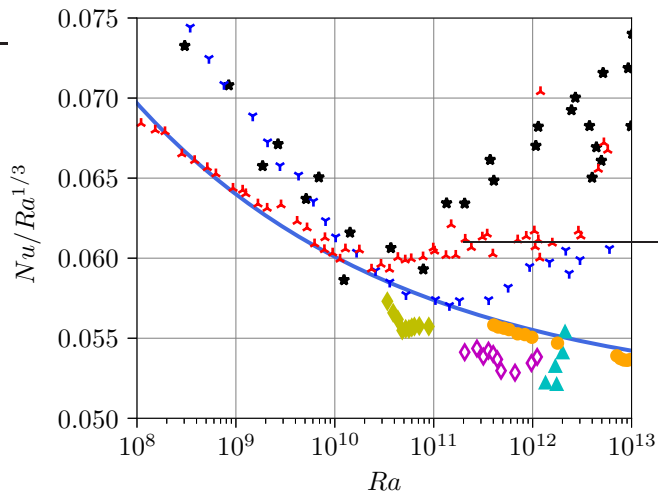


Fig. 1: Heat transfer measurements in FC770 (present work) in the $\Gamma = 2$ cell (yellow diamonds) and in the $\Gamma = 1$ cell (open magenta diamonds at 25 °C, and cyan triangles at 40 °C). Several high-Rayleigh number heat-transfer measurements are shown for reference: the heat-transfer from Chavanne, et al. [16] ($\Gamma = 1/2$) in black stars, from He, et al. [14] ($\Gamma = 1$) in orange circles, from Niemela, et al. with $\Gamma = 1$ [17] in blue 3-branch stars and $\Gamma = 4$ [18] in red 3-branch stars. Solid lines: estimates from the Grossmann-Lohse model with the updated prefactors [15], for $Pr = 14$.

inar $\epsilon \sim Re^{5/2}$ regime to a turbulent $\epsilon \sim Re^3$ regime; (ii) a change in the statistics of the temperature fluctuations. The latter was later confirmed with a smaller thermometer [20]. In the following, we focus on velocity measurements, and estimates of the dissipation, to compare the dissipation scaling with the scaling in cells with and without heat-transfer enhancement.

Shadowgraph and velocity measurement. – In this range of Rayleigh numbers, the wind velocity is often estimated from the correlations of local thermometers [10, 11, 16, 21, 22]. In this work, we use optical methods which allow to resolve the velocity field. However, the cost of FC770 as a working fluid makes it unsuitable to particle seeding, as pollution of the working fluid would be very costly. Therefore, we based the measurements on shadowgraph, which is non-invasive and does not pollute the working fluid.

The set-up is the similar to the one described in [12], and consists in direct shadowgraphy in diverging light. In this paper, the cell is illuminated by a punctual monochromatic light (M450LP1 LED from ThorLabs). The light source is far enough from the cell, that the light is almost parallel. The shadowgraph pattern is captured on a ground glass diffuser, and recorded with a PCO Pandas camera, with a resolution 2048×2048 . An example of shadowgraph pattern is shown in figure 2.

There are several strategies to infer an estimate of the velocity fields from the shadowgraph images. In a previous work, we investigated a simple method based on

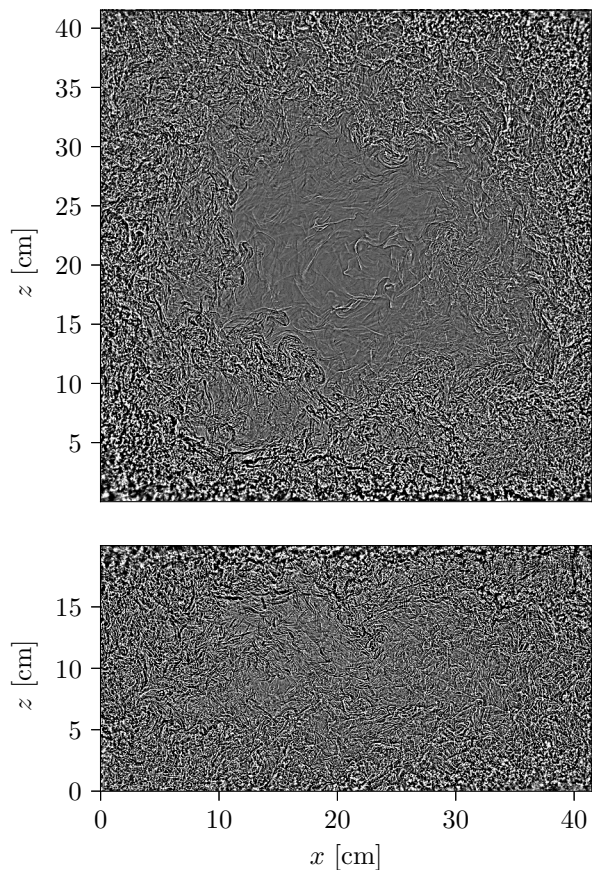


Fig. 2: Shadowgraph image in the Rayleigh-Bénard cell with FC770. Top: Aspect ratio 1 cell at $Ra = 1.3 \times 10^{12}$ (40 °C). Bottom: Aspect ratio 2 cell at $Ra = 8.9 \times 10^{10}$ (25 °C).

space-time diagrams [12]. Because this method tracks the plumes, it allows to infer statistics on the plumes. However, the drawback is that the measurement is averaged over lines. In the present work, we investigate an alternative method which consists in applying to the shadowgraph pattern the same algorithm that we use for Particle Image Velocimetry (PIV), i.e. Correlation Image Velocimetry (CIV) from the CIVx toolbox implemented by Fincham and Delerce [23].

This is possible in this range of Rayleigh numbers, because plumes are relatively small and fill the entire volume, and therefore may act as local pattern for the correlation algorithm similar to the particles in PIV. One important difference between the velocity field obtained in this way compared to the velocity field in PIV is that the light pattern is integrated over the depth of the cell, while particles in PIV are imaged on a light sheet. In our case, however, the flow is quasi bi-dimensional, so the integration across the depth does not blur excessively the flow field. To validate the method, we applied it to the case of deionized water, for which we could compare against PIV measurement. As can be seen in Figure 3, the average flow pattern is well recovered, except in the corners

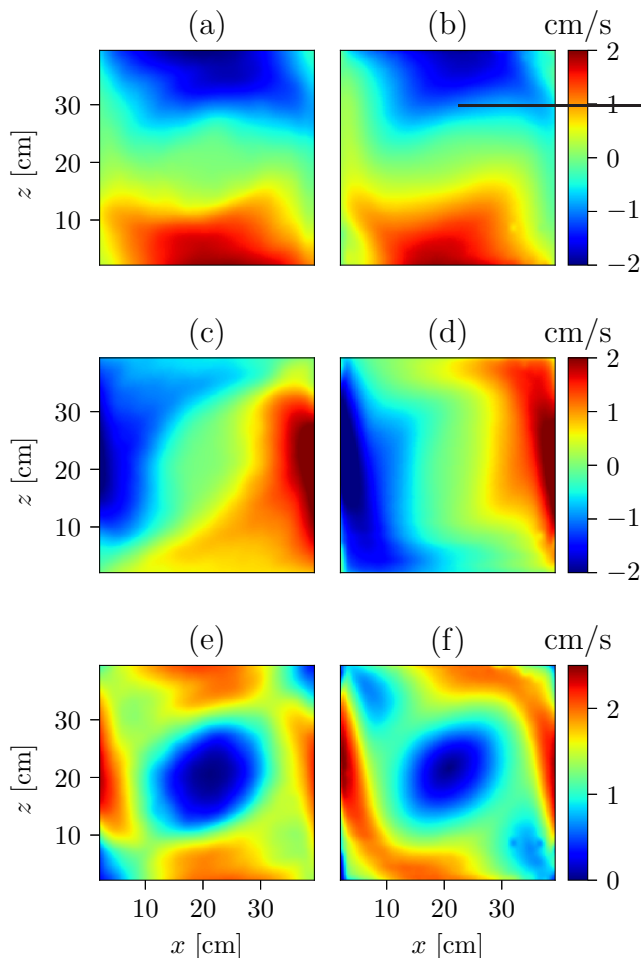


Fig. 3: Right column: velocity field obtained by Liot, *et al.* [5] using Particle Image Velocimetry (PIV) at $Ra = 6.9 \times 10^{10}$ and $Pr = 4.4$ in water. Left column: velocity field obtained from Correlation Image Velocimetry from the Shadowgraph pattern (present work) in the same cell and same Ra and Pr . (a, b) mean horizontal component U , (c, d) mean vertical component V , (e, f) mean velocity magnitude $\sqrt{U^2 + V^2}$.

where both upwelling and downwelling plumes are visible on the Shadowgraph sequence, which results in small velocity magnitude in the CIV field.

Reynolds number and friction coefficient. – There are different kinds of definitions for the Reynolds number in the literature: based on the average velocity, the average turnover time, or the velocity fluctuations. The position of the sensor also varies, which makes it difficult to directly compare the value of the Reynolds numbers. However, Musilovà, *et al.* have compared estimates based on the sloshing mode frequency, time of flight between thermometers, and average or fluctuating velocities from the Elliptic approximation, and found that all these estimates roughly scale identically [11].

In the following, we use the vertical component of the velocity inside the jet. From the mean velocity field, we

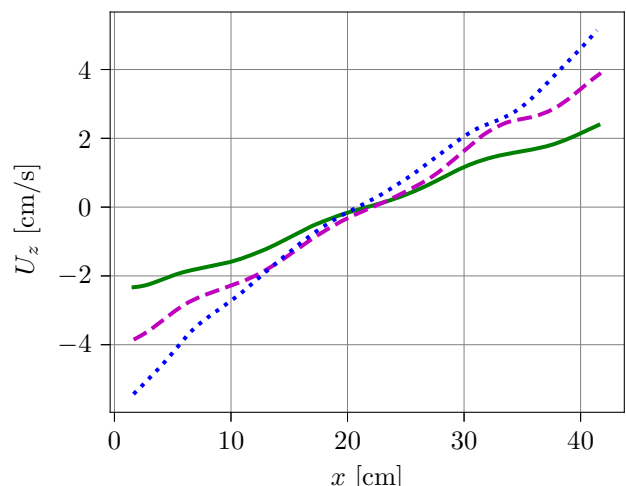


Fig. 4: Velocity profiles at mid-height in the $\Gamma = 1$ cell with FC770 as the working fluid. Solid green line: $Ra = 3.6 \times 10^{11}$, dashed purple line: $Ra = 9.7 \times 10^{11}$, dotted blue line: $Ra = 2.1 \times 10^{12}$.

compute velocity profiles at mid-height, by spatially averaging on a window of height 2 cm. Examples of velocity profiles are shown in Figure 4. We use the maximum of these velocity profiles to compute the Reynolds number. They are given in Table 2. As can be seen in Figure 5, they are in fair agreement with other Reynolds number data from the literature, with a scaling close to $Ra^{1/2}Pr^{-0.7}$.

Let us recall that the balance of kinetic energy yields the following exact relation [1, 2],

$$\epsilon = \frac{\nu^3}{h^4} (Nu - 1) Ra Pr^{-2}, \quad (6)$$

where ϵ is the kinetic energy dissipation rate. In the developed turbulence limit, one may expect $\epsilon \sim \frac{U^3}{h} \propto Re^3$. The non dimensional ratio,

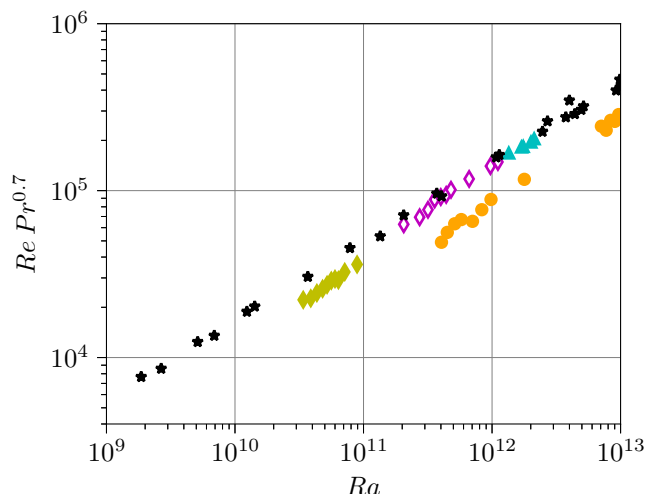
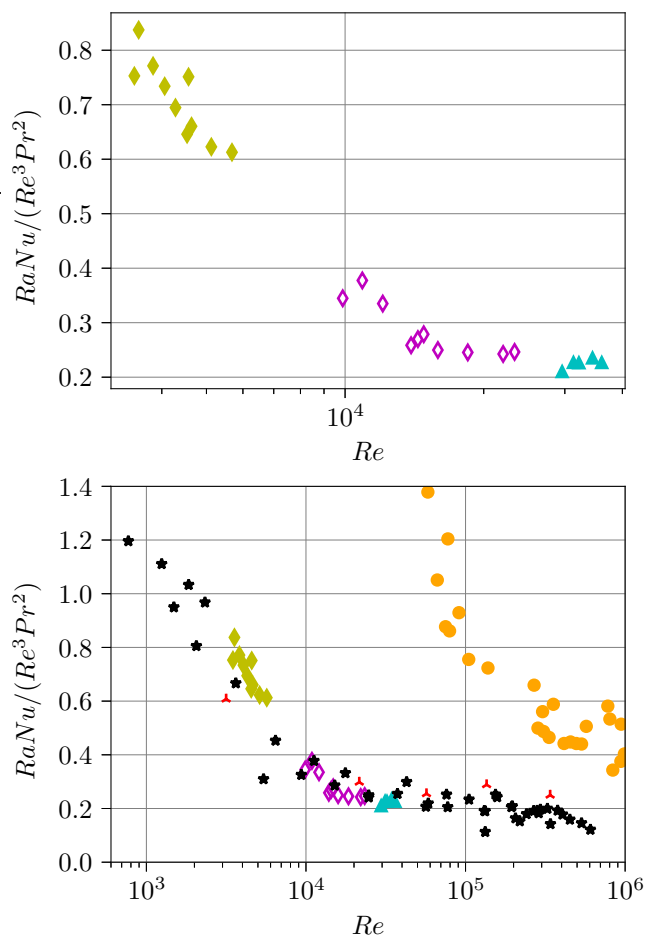
$$\frac{(Nu - 1) Ra Pr^{-2}}{Re^3} = \frac{\nu(\text{grad } \mathbf{u})^2}{u^3/h}, \quad (7)$$

is similar to a friction coefficient, and scales like $1/\sqrt{Re}$ at low Reynolds number (viscous limit), and features a plateau in the high Reynolds number limit.

As can be seen in Figure 6, the friction coefficient in the FC770 experiment reaches a plateau at the highest forcing (at Rayleigh numbers larger than 10^{12}). In addition, the value of the plateau is in quantitative agreement with the results from Chavanne, *et al.* [16] and Niemela, *et al.* [10, 17]. We may note also that the recent data from Musilovà, *et al.* [11] are also in quantitative agreement with those of Niemela, *et al.* The data from He, *et al.* [14, 22] also features a plateau, but only at their highest forcing. They are slightly offset compared to the other measurements, but this is of no consequence. Indeed, it may be caused by their slightly lower Reynolds numbers, possibly resulting from the choice of the thermometer positions. In principle,

Table 2: Heat-transfer and mean velocity non-dimensional values in both cells, using FC770 (Pr between 11 and 14) as working fluids.

Ra	Nu	Re	Pr	Γ
3.4×10^{10}	185.6	3487	14.1	2
3.9×10^{10}	191.7	3563	14.1	2
4.3×10^{10}	197.3	3829	14.1	2
4.8×10^{10}	201.7	4058	14.1	2
5.2×10^{10}	207.5	4283	14.1	2
5.6×10^{10}	212.8	4539	14.1	2
6.0×10^{10}	217.9	4641	14.1	2
6.4×10^{10}	222.7	4572	14.1	2
7.1×10^{10}	231.4	5124	14.1	2
8.9×10^{10}	248.9	5681	14.1	2
2.1×10^{11}	319.5	9882.8	14.1	1
2.7×10^{11}	352.8	10900	14.1	1
3.2×10^{11}	367.3	12073	14.1	1
3.6×10^{11}	384.8	13908.9	14.1	1
4.0×10^{11}	397.7	14391	14.1	1
4.4×10^{11}	408.2	14818	14.1	1
4.8×10^{11}	414.5	15904	14.1	1
6.6×10^{11}	460.9	18469	14.1	1
9.7×10^{11}	529.3	22038	14.1	1
1.1×10^{12}	557.5	23338	14.1	1
1.7×10^{12}	627.9	31321	12.5	1
1.3×10^{12}	576.9	29597	11.9	1
1.7×10^{12}	634.7	32186	11.9	1
2.0×10^{12}	682.4	34454	11.9	1
2.1×10^{12}	712.3	36082	11.9	1


 Fig. 5: Reynolds number measurement with FC770 (present work) in the $\Gamma = 2$ cell (yellow diamonds) and in the $\Gamma = 1$ cell (open magenta diamonds at 25 °C, and cyan triangles at 40 °C). For reference: Reynolds number from Chavanne, et al. [16] (black stars) and from He, et al [22] (orange circles).

 Fig. 6: Friction coefficient *versus* the Reynolds number. Top: data with the FC770 (present work). $\Gamma = 1$, solid cyan triangles (40 °C), solid yellow diamonds (25 °C). $\Gamma = 2$, open purple diamond (25 °C). Bottom: comparison with friction coefficient from the literature. Black star from Chavanne, et al. [16], red 3-branch stars from Niemela, et al. [10] at aspect ratio 1, orange circles from He, et al. [14, 22].

and unlike intrinsic estimates such as the Taylor microscale Reynolds number R_λ , all Reynolds number estimates which are based on large scale quantities are defined with a $O(1)$ prefactor. The important point is that they reach the friction *versus* Re plateau, but only at their highest forcing, which is consistent with their transition observed at higher Rayleigh number compared to Chavanne, et al.

This seems to indicate that the transition to the “ultimate regime” may be controlled by the Reynolds number rather than the Rayleigh number. Although all experiments show a similar Ra versus Re scaling, one must not forget the Pr dependency, as well as possible dependencies on the geometry and flow configurations. Therefore, a threshold on the Reynolds number does not translate into a threshold on the Rayleigh number. Additionally, while the plateau is clearly visible on the present FC770 data, there is no visible heat-transfer enhancement. The

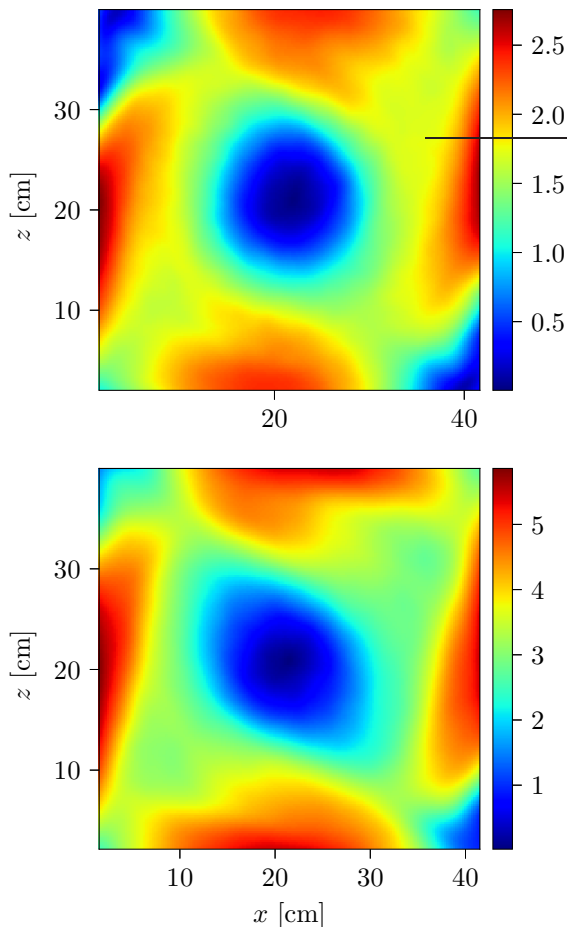


Fig. 7: Velocity fields in the $\Gamma = 1$ cell with FC770. Top: $Ra = 3.6 \times 10^{11}$ (25 °C). Bottom: $Ra = 2.1 \times 10^{12}$ (40 °C).

reason is that our data lies at the beginning of the friction plateau, and the transition on the Nusselt number is not very sharp.

However, as can be seen in Figure 7, the structure of the large scale circulation (LSC) is identical on the full range of Rayleigh numbers that can be obtained in the cell with FC770. It is also similar to the velocity field obtained in water (see Fig 3) at lower Rayleigh numbers, and in fair agreement with the LSC structure reported by Xia, Sun & Zhou [4] at $Ra = 3.5 \times 10^{10}$. They report however a change from an oval-shaped LSC to the same rectangular-shaped LSC that we observe, at a threshold Rayleigh number of order 10^{10} . The present work indicates that this rectangular-shaped LSC is very robust and remains unchanged up to $Ra = 2 \times 10^{12}$, in a range where the scaling of the kinetic dissipation rate is compatible with the turbulent regime.

Additionally, as shown in Fig 8, in the high Reynolds number limit, it seems that all Nusselt number data can be fairly well collapsed with the phenomenological scaling,

$$Nu \sim Re^{0.8} Pr^{0.6}. \quad (8)$$

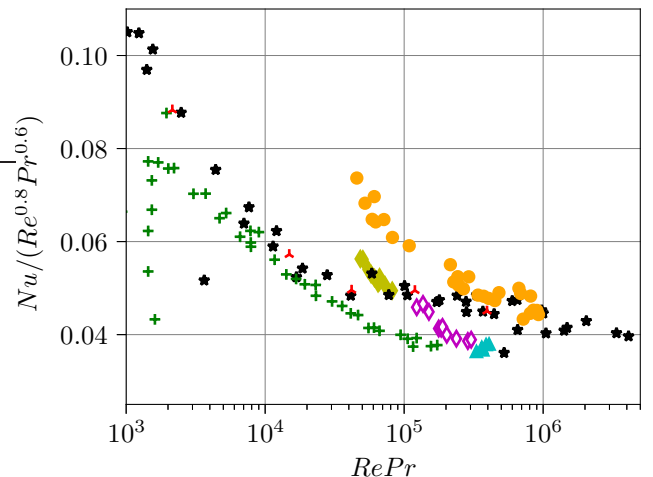


Fig. 8: Compensated Nusselt number as a function of the Péclet number, $Pe = RePr$. When the data gets to a plateau, the scaling is $Nu \sim Re^{0.8} Pr^{0.6}$. The symbols are identical to previous figures, with the addition of the data from Wu Ph.D. thesis [24] (green crosses).

More precisely, it seems that the threshold is controlled by the Péclet number, $Pe = RePr$, rather than the Reynolds number, and occurs for a Péclet number of order 10^5 . This is somewhat consistent with the analysis of Kraichnan [19].

Conclusion. – We showed that the flow in our cell undergoes a transition to a turbulent regime, where the kinetic energy dissipation scales like Re^3 , and the Nusselt number is a universal function of the Reynolds and Prandtl numbers. One possible reason for the apparent discrepancy in the literature is that the transition is controlled by the Péclet number. This might also explain why Roche finds that there is a Ra -dependant transition threshold for the Prandtl number [21]. Indeed, the measurements in SF_6 have a nearly constant Prandtl number of order 0.8, almost ten times lower than the Prandtl number in the high Rayleigh numbers data of Chavanne, et al. As can be seen in Fig 8, they reach similar Péclet number only at their higher forcing.

While the scaling of the Reynolds number with the Rayleigh number is quite robust, the effective Reynolds number may still differ, for a given Ra , in one experiment, compared to another experiment. This discrepancy may be due to the Prandtl number, effects of the geometry, or the actual flow configuration. In addition, it is not possible to define the Reynolds number in a universal way, in a flow which is neither isotropic nor homogeneous. That makes comparison of transition thresholds between experiments intrinsically challenging.

Yet, the intensity of the LSC does not seem to change in the turbulent regime, and the scaling of the Reynolds number is not significantly modified beyond the turbulent transition. This is consistent with the observations of Roche, et al. [21], which showed that the transition in Grenoble

did not feature a dramatic change in the LSC either. It is particularly striking that the scaling of the Reynolds number versus Rayleigh number is incredibly consistent across all experiments, whether or not they feature a transition to an enhanced heat transfer regime.

One possible mechanism is that the transition is really triggered by the fluctuations, or boundary eddies as suggested by Roche [25]. It is likely that the velocity fluctuations may scale similarly to the average velocity, at least up to the turbulent transition, which might explain why the Reynolds number based on the LSC intensity still acts as a good parameter. It would therefore be very useful to study in more details the velocity fluctuations, and the small scale structures near the boundary, below and above the turbulent transition. Remarkably, in the case of convection cells with rough boundaries, we did find also that the intensity of the LSC was not changed above and below the roughness-triggered transition to enhanced heat transfer regime, but that the intensity of velocity fluctuations, as well as the statistical features, were indeed significantly enhanced [5].

* * *

We are very grateful to M'hamed Boutaous, Hervé Pabiou and the staff at CETHIL laboratory for their help with the measurement of the fluid thermal properties. This work was funded by ANR-18-CE30-0007-01 JCJC "CryoGrad" project, and benefited from the resources of the PSMN computing centre in Lyon. We warmly thank Marc Moulin and the mechanical workshop for the design and setup of the experimental apparatus. We thank Bernard Castaing and Philippe Roche for stimulating discussions.

REFERENCES

- [1] Ahlers G, Grossmann S and Lohse D 2009 *Rev. Mod. Phys.* **81** 503
- [2] Chillà F and Schumacher J 2012 *Eur. Phys. J. E* **35** 58
- [3] Qiu X L and Tong P 2001 *Phys. Rev. E* **64** 036304
- [4] Xia K Q, Sun C and Zhou S Q 2003 *Phys. Rev. E* **68** 066303
- [5] Liot O, Ehlinger Q, Rusaouën E, Coudarchet T, Salort J and Chillà F 2017 *Phys. Rev. Fluids* **2** 044605
- [6] Ni R, Huang S D and Xia K Q 2012 *J. Fluid Mech.* **692** 395–419
- [7] Liot O, Gay A, Salort J, Bourgoïn M and Chillà F 2016 *Phys. Rev. Fluids* **1** 064406
- [8] Sano M, Wu X Z and Libchaber A 1989 *Phys. Rev. A* **40** 6421–6430
- [9] Chavanne X, Chillà F, Castaing B, Hébral B, Chabaud B and Chaussy J 1997 *Phys. Rev. Lett.* **79** 3648–3651
- [10] Niemela J J, Skrbek L, Sreenivasan K R and Donnelly R J 2001 *Journal of Fluid Mechanics* **449** 169–178
- [11] Musilová V, Králik T, Mantia M L, Macek M, Urban P and Skrbek L 2017 *J. Fluid Mech.* **832** 721–744
- [12] Belkadi M, Guislain L, Sergent A, Podvin B, Chillà F and Salort J 2020 *J. Fluid Mech.* **895** A7
- [13] Xie Y C and Xia K Q 2017 *J. Fluid Mech.* **825** 573–599
- [14] He X, Funfschilling D, Bodenschatz E and Ahlers G 2012 *New J. Phys.* **14** 063030
- [15] Stevens R J A M, van der Poel E P, Grossmann S and Lohse D 2013 *J. Fluid Mech.* **730** 295–308
- [16] Chavanne X, Chillà F, Chabaud B, Castaing B and Hébral B 2001 *Phys. fluids* **13** 1300–1320
- [17] Niemela J J and Sreenivasan K R 2003 *J. Fluid Mech.* **481** 355–384
- [18] Niemela J and Sreenivasan K 2006 *J. Fluid Mech.* **557** 411–422
- [19] Kraichnan R H 1962 *Phys. Fluids* **5** 1374–1389
- [20] Gauthier F, Salort J, Bourgeois O, Garden J L, du Puits R, Thess A and Roche P E 2009 *EPL* **87** 44006
- [21] Roche P E, Gauthier F, Kaiser R and Salort J 2010 *New J. Phys.* **12** 085014
- [22] He X, van Gils D P M, Bodenschatz E and Ahlers G 2015 *New J. Phys.* **17** 063028
- [23] Fincham A and Delerce G 2000 *Exp. Fluids Suppl.* **29** S13–S22
- [24] Wu X Z 1991 *Along a road to developed turbulence : free thermal convection in low temperature Helium gas* Ph.D. thesis University of Chicago
- [25] Roche P E 2020 *New J. Phys.* **22** 073056